Geophysical Journal International

Geophys. J. Int. (2011) doi: 10.1111/j.1365-246X.2010.04914.x

Mapping spherical seismic into physical structure: biases from 3-D phase-transition and thermal boundary-layer heterogeneity

Elinor Styles, D. Rhodri Davies and Saskia Goes

Department of Earth Science and Engineering, Imperial College London, UK. E-mail: elinor.styles03@imperial.ac.uk

Accepted 2010 December 2. Received 2010 December 1; in original form 2010 October 2

SUMMARY

Earth's mantle is, to a very good first approximation, spherically symmetric, with lateral deviations in seismic velocities and density of only a few per cent. This observation has led to the common assumption that average radial seismic models reflect the mantle's average physical structure. We test this assumption by using a set of dynamically generated mantle structures and comparing seismic velocities for the average radial physical state with laterally averaged seismic velocities. The thermal and thermochemical dynamic circulation models are Earth-like in terms of convective vigour, thermal structure and geographical pattern of heterogeneity. We find that, in general, averaged seismic structure is not distinguishable from the seismic structure of the physical average, within the uncertainty bounds of seismic reference models. An exception is near phase boundaries, where phase-boundary topography broadens the averaged seismic jump relative to the discontinuity at physical reference conditions. In an inversion for 1-D seismic structure, where narrow discontinuities are imposed, these biases may map into a lower jump, and substantially stronger velocity gradients above and below the interface than are actually present. Other small biases in averaged structure occur in thermal boundary layers, including those that form above chemical piles. These biases are caused by large lateral variations in temperature, not compositional variability.

Key words: Elasticity and anelasticity; Phase transitions; Seismic tomography; Dynamics of lithosphere and mantle.

1 INTRODUCTION

Seismic inversions generally map structure in terms of anomalies relative to global 1-D reference models, such as PREM (Dziewonski & Anderson 1981) and AK135 (Kennett *et al.* 1995). The reference models explain over 90 per cent of the seismic signal, but the few per cent lateral deviations reflect Earth's internal dynamics (e.g Montagner 1994; Trampert & van der Hilst 2005). To make meaningful physical interpretations of these 3-D anomalies, we need to know what thermal and compositional structure the reference models represent.

Previous studies that forward modelled seismic 1-D structure reached different conclusions on the mantle's background structure, ranging from purely thermal at adiabatic, sub- or super-adiabatic conditions, to a mantle that varies in composition with depth (Anderson & Bass 1986; Bina & Silver 1990; Jackson & Rigden 1998; da Silva *et al.* 2000; Deschamps & Trampert 2004; Mattern *et al.* 2005; Matas *et al.* 2007; Cobden *et al.* 2008; Irifune *et al.* 2008; Khan *et al.* 2008; Mao *et al.* 2008; Cobden *et al.* 2009). The most popular model is that of an adiabat with a potential temperature of around 1300 °C and a constant pyrolitic composition, thus satisfying the conditions necessary for Mid Ocean ridge basalt (MORB) generation. Furthermore, isochemical and adiabatic/slightly subadiabatic conditions would prevail if the mantle, as a whole, was convectively well mixed.

While adiabatic pyrolite provides a good match to several 1-D seismic model characteristics (Ringwood 1962; Weidner 1985; Ita & Stixrude 1992; Jackson & Rigden 1998; Li & Liebermann 2007, Fig. 1) there are discrepancies in fine detail (e.g. Anderson & Bass 1986; Duffy & Anderson 1989; Li *et al.* 1998; Irifune *et al.* 2008; Mao *et al.* 2008). Although some of these discrepancies may be within the uncertainties associated with the seismic models or equation of state parameters used to map physical into seismic structure (Jackson 1998; Kennett & Jackson 2009), others appear to exceed them (Cammarano *et al.* 2005a,b; Cobden *et al.* 2008, 2009). These include the magnitude of the jump in seismic velocity at 410 km depth and upper-mantle velocity-depth gradients. Such discrepancies, and the fact that it is difficult to reconcile constraints from *P* and *S* velocities simultaneously with a single physical reference structure, have led to the large range of alternative interpretations.

Whole mantle convection, incorporating phase transitions and compositional variations in buoyancy, can lead to complex and potentially large-scale structures, thus generating variations in averaged composition with depth (McNamara & Zhong 2004; Tackley *et al.* 2005). This raises the possibility that averaged seismic structure does not reflect the averaged physical structure, owing to the

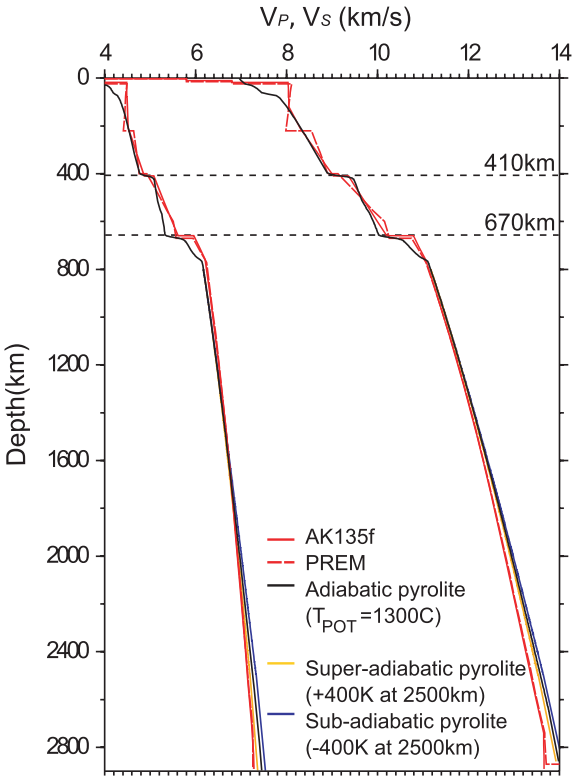

Figure 1. Two 1-D seismic reference models (AK135 and PREM) (Dziewonski & Anderson 1981; Kennett *et al.* 1995), compared with the velocities corresponding to a pyrolitic mantle along a 1300 °C adiabat, and along profiles with lower-mantle sub- and super-adiabatic conditions. No tested thermal structure can reproduce the fine detail of either reference model in the upper mantle, or reconcile lower mantle V_P and V_S.

non-linear sensitivity of seismic velocities to temperature and composition (Kennett 2006; Cobden *et al.* 2008, 2009).

In this study, we investigate the potential for such 'bias', using a series of global 3-D spherical mantle circulation models, which span a range of plausible thermal and compositional mantle structures. Modelled temperature, pressure and composition (T, P, X) is converted into seismic velocities (V_P, V_S, V_Φ) using a thermodynamic approach. Subsequently, horizontally averaged seismic structure, $<V(T, P, X)>$, is compared with the seismic structure expected for the physical average, $V<(T, P, X)>$, to determine whether any systematic differences occur. Additional biases may be introduced by uneven seismic data coverage and seismic inversion methods (Mégnin *et al.* 1997; Bunge & Davies 2001; Davies & Bunge 2001; Kennett 2006; Ritsema *et al.* 2007). However, determining how these map into a 1-D structure requires further work, which is beyond the scope of this paper.

2 CONVECTION MODEL

We generate a global (T, P, X) field using a modified and benchmarked version of TERRA, a well-known mantle convection code that solves the conservation equations of mass, momentum and energy at infinite Prandtl number (Stokes flow) in a spherical shell, with the inner radius being that of the outer core and the outer radius corresponding to Earth's surface (Baumgardner 1985; Bunge *et al.* 1997; Davies & Davies 2009). We employ a mesh with over 80 million discrete nodal points, thus providing the fine resolution necessary to explore mantle flow at Earth-like convective vigour.

Our models incorporate compressibility, in the form of the anelastic liquid approximation (Jarvis & McKenzie 1980). Radial reference values are represented through a Murnaghan equation of state (Murnaghan 1951), with parameter values identical to Bunge *et al.* (2002). Isothermal temperature boundary conditions are prescribed (300 K—surface; 4000 K—core–mantle boundary, hereafter CMB), while the mantle is also heated internally. Surface velocities are assimilated according to 230 Myr of plate motion history (Stampfli & Borel 2002; Stampfli & Borel 2004; Stampfli & Hochard 2009) while a free-slip boundary condition is specified at the CMB. Phase changes are incorporated at 410- and 660-km depth, as sheet mass anomalies (Tackley *et al.* 1993). Depth-dependent viscosity is included, increasing in the lithosphere and lower mantle by factors of 10 and 100, respectively. In addition, viscosity varies with temperature by a factor of 200. For a summary of key model parameters, see Table 1.

For our initial conditions, we run a standard convection model (i.e. free-slip surface boundary) until a thermal quasi-steady state is achieved. We then follow a similar philosophy to Bunge *et al.* (2002) and approximate the unknown initial conditions of early Triassic mantle heterogeneity by running our models with global plate configurations fixed to the oldest available reconstruction at 230 Ma, for ∼100 Myr. Thermochemical models are initiated with a 700-km thick basal layer of dense material, which progressively deforms as the model evolves. Note that in this study, the buoyancy number is defined as $B = \Delta\rho_C/\Delta\rho_T$, where $\Delta\rho_T = \alpha_s\rho_s\Delta T_s$, α_s and ρ_s are the thermal expansion and density at the surface, while ΔT_s is the super-adiabatic temperature difference from surface to CMB.

We examined over 50 models in total, but focus on three here (Figs 2–5):

(1) Model T: an isochemical model, heated 65 per cent internally and 35 per cent through its base (CMB heating ratio = 0.35). The model has boundary layers of ∼100 km thickness, with the upper-mantle planform dominated by strong downwellings in regions of present-day plate convergence (Fig. 2). In the lower mantle, remnants of older subduction are visible, while concentrations of hot upwellings are located under the Pacific and Africa, owing to the strong core heat flux (Schuberth *et al.* 2009). The radially averaged temperature profile (Fig. 5a) is slightly subadiabatic. Lateral temperature anomalies amount to a few hundred degrees only and

Table 1. Parameters common to all models. Rayleigh numbers are calculated from reference equation of state parameters at the Earth's surface and the reference viscosity. Radial reference values are represented through a Murnaghan (1951) equation of state, with parameter values as in Bunge *et al.* (2002).

Parameter	Value
Ra (b)	$\sim 6 \times 10^7$
Ra (h)	$\sim 8 \times 10^8$
Reference viscosity	1.5×10^{21} Pa s
Viscosity jump at 100, 600 km	0.1, 100
E (pre-exponential factor for η_T)	5.298
$T_{\rm surf}$, $T_{\rm CMB}$	300 K, 4000 K
Cl_{410}, Cl_{660}	+3.0 M Pa K^{-1}, −2.0 M Pa K^{-1}
Thermal conductivity	4.0 W m^{-1} K^{-1}
Thermal expansivity surface	4.0×10^{-5} K^{-1}
Thermal expansivity CMB	1.2×10^{-5} K^{-1}
Internal heating rate	5.0×10^{-12} W kg^{-1}
Heat capacity	1.1×10^3 kg^{-1} K^{-1}

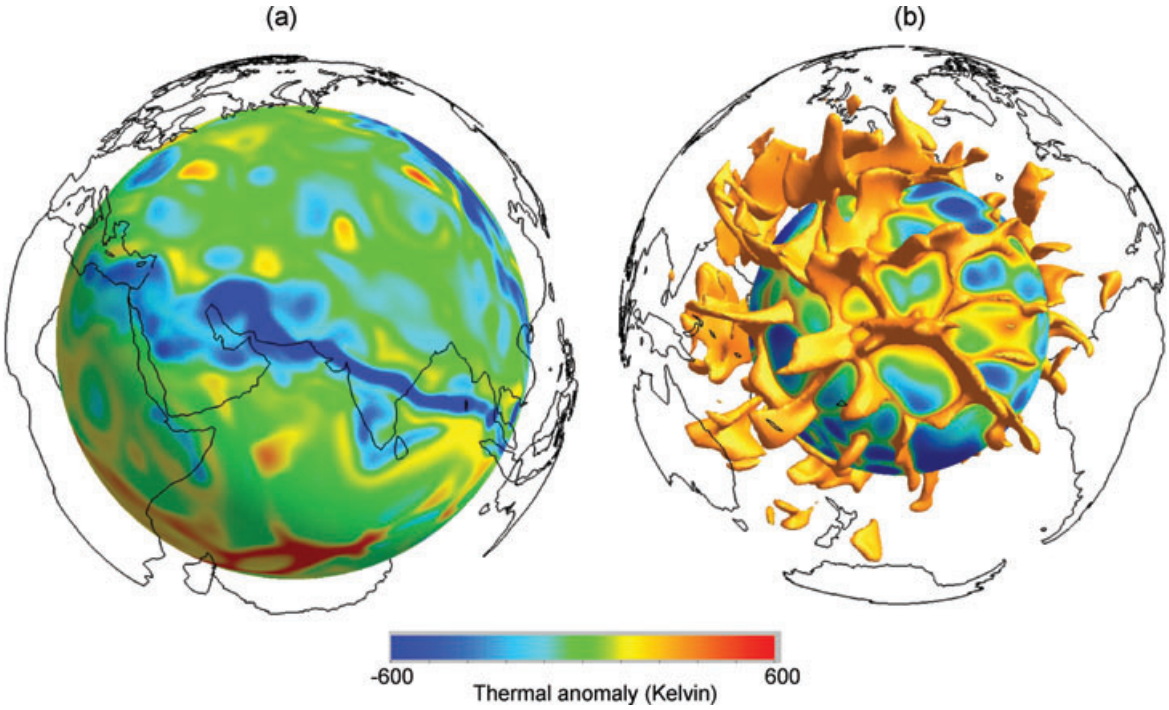

Figure 2. The thermal field from Case T. The scale illustrates the temperature, away from the layer average (i.e. the thermal anomaly): (a) includes a radial surface at 1000 km depth from a view centred on the Arabian Sea, whilst (b) shows a view centred on the Pacific that includes a radial surface at 2800 km depth and an isosurface, representing regions of the mantle that are 300 K hotter than average for their depth. In this, and all other models examined herein, the upper-mantle planform is dominated by strong downwellings in regions of present-day plate convergence. In the mid and lower mantle, remnants of older subduction are visible, illustrated here for the Tethyan region (a). In addition, concentrations of hot upwellings are located under the Pacific (b) and Africa, in regions that are devoid of recent subduction.

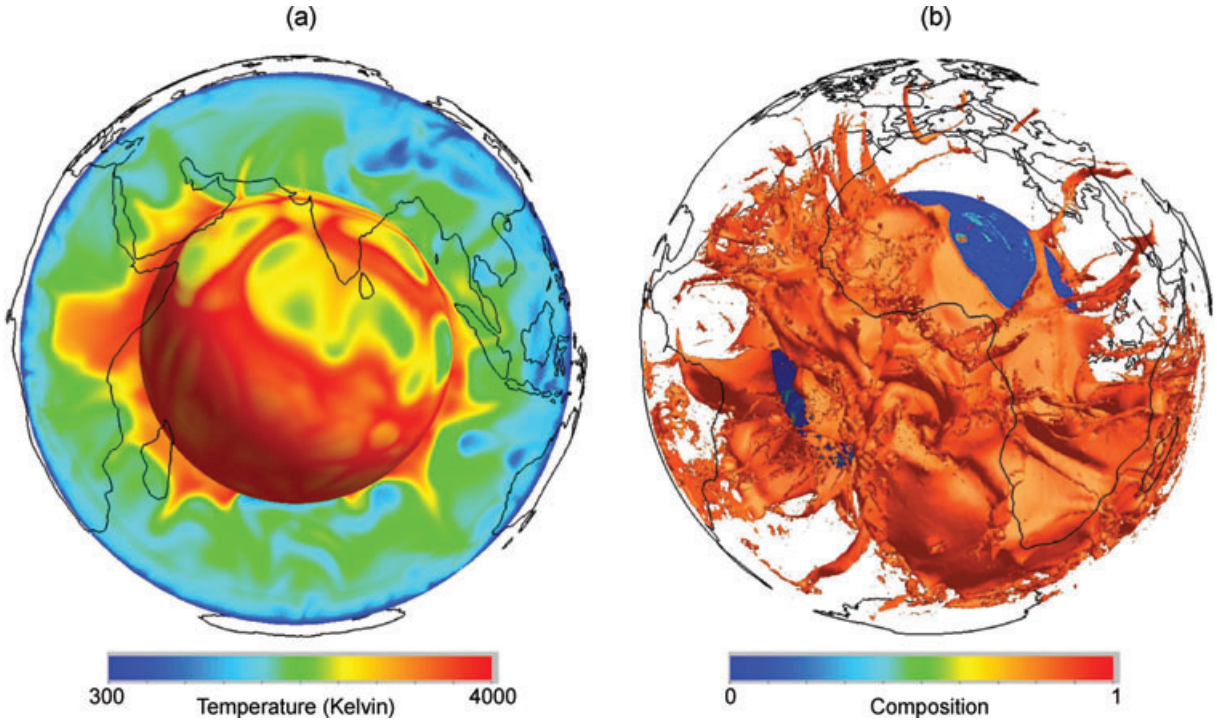

Figure 3. The structure of thermochemical case TC2.5: (a) a snapshot of the thermal field showing a radial surface at 2800 km depth and a cross section from an Indian Ocean perspective; (b) layer topography mapped by the $X = 0.9$ isosurface from an Atlantic/African perspective. Substantial lower-mantle temperature anomalies are observed, owing to the presence of dense chemical piles, which concentrate beneath Africa and the Pacific.

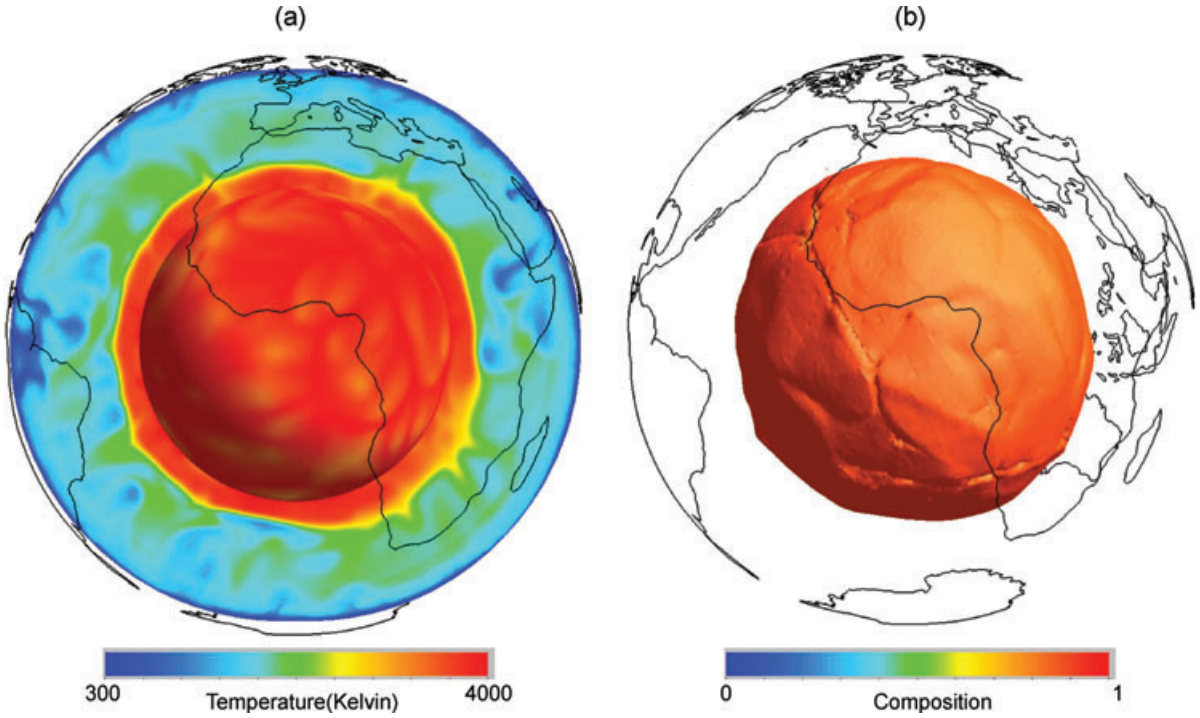

Figure 4. The structure of thermochemical case TC5.0: as in Fig. 3, the thermal field is shown in (a) and a compositional $X = 0.9$ isosurface in (b) both from an Atlantic/African perspective. Substantial excess temperatures build up below the globally continuous chemical interface. There is no significant entrainment of dense material across this interface.

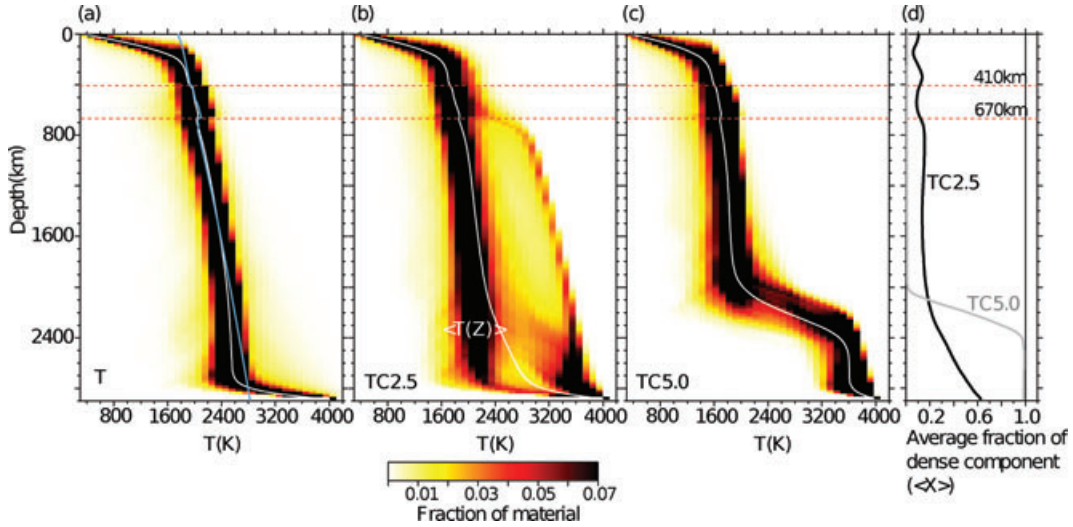

Figure 5. For the three dynamic models, (a)–(c) show temperature distribution and (d) average radial volume fraction of the dense component, X. For reference an adiabatic temperature profile with potential temperature of 1400 °C (solid blue line) is shown in Panel a. The models represent end-member scenarios for the Earth's mantle.

increase with depth, as expected for a vigorously convecting system with substantial internal heating (e.g. Bunge *et al.* 2001).

(2) Model TC2.5: a thermochemical model (CMB heating ratio = 0.29), where the initial basal layer has an excess density of 2.5 per cent ($B \cong 0.25$): a lower bound for suggested common heterogeneities (e.g. from recycled slabs). The model evolves to form a strongly undulating interface, dominated by locally discontinuous chemical piles. Hot dense material is focussed beneath Africa and the Pacific and spreads throughout the lower-mantle depth range (Fig. 3). Downwellings are of similar morphology to those of Model T. The radial temperature profile is super-adiabatic, owing to the large excess temperatures of dense chemical piles (Figs 5b or d).

(3) Model TC5.0: a thermochemical model (CMB heating ratio = 0.12), where the dense component has an excess density of 5.0 per cent ($B \cong 0.5$): a maximum value for plausible dense-layer compositions. A globally continuous layer forms, with upwelling plumes rising from a strong thermal boundary layer above the chemical interface (Fig. 4). As in Model TC2.5, the radial temperature profile is super-adiabatic (Figs 5c or d).

Table 2. Major-oxide composition (in mol per cent) of the three compositions used in this study.

	Oxide (mol per cent)				
	SiO_2	MgO	Al_2O	FeO	CaO
Pyrolite (Sun 1982)	38.61	49.13	2.77	6.24	3.25
MORB (Perrillat *et al.* 2006)	53.82	13.64	10.13	8.8	13.6
Fe-rich chondrite (Anderson 1989)	40.03	43.37	1.68	11.68	3.24

All models are Earth-like in terms of convective vigour, thermal structure, surface heat flux and the geographic pattern of heterogeneity (controlled by the assimilated plate motion history). More complete formulations of rheology, thermal expansion and compressibility as a function temperature, depth and composition, as well as the inclusion of transitions in non-olivine components, are important to understand the full dynamics and evolution of the system (Ita & King 1994, 1998; Mambole & Fleitout 2002; Tackley *et al.* 2005; Tan & Gurnis 2007; Deschamps & Tackley 2008, 2009). However, our model set-up is sufficiently realistic to represent plausible end-member structures in terms of the distribution of thermal and compositional heterogeneities. Our results span a wide range of competing conceptual mantle models (Tackley 1998; Kellogg *et al.* 1999; Tackley 2002; Davaille *et al.* 2003; McNamara & Zhong 2004; Deschamps & Tackley 2008, 2009; Schuberth *et al.* 2009; Simmons *et al.* 2009).

3 CONVERSION INTO SEISMIC VELOCITIES

The modelled (T, P, X) fields are converted into seismic velocities following Cobden *et al.* (2008, 2009). We use a thermodynamic approach (Stixrude & Lithgow-Bertelloni 2005) to calculate self-consistently phase equilibria, density and elastic parameters, with the code PerPleX (Connolly 2005), for the CFMAS database 'sfo05' (Stixrude & Lithgow-Bertelloni 2005; Khan *et al.* 2006) and correct for the effects of temperature- and frequency-dependent anelasticity (model Q4 Goes *et al.* 2004). These choices provide average sensitivity to T, P and X, within the range of mineral-physics uncertainties. Calculations with alternative databases and different anelasticity formulations (Cobden *et al.* 2008, 2009) give very similar results in terms of biases to the 1-D models.

Three compositions are explored (Table 2): pyrolitic for the background mantle, and either a basaltic (representative of subducted material) or Fe-rich chondritic composition (as a potential dense primitive material) for the dense component. These high-density compositions (both 3 ± 0.5 per cent denser than pyrolite) have distinct seismic signatures; the basaltic composition being generally faster and the Fe-rich composition generally slower, than a pyrolite. Other melt-depleted, peridotitic or chondritic compositions have similar velocities to pyrolite, although with some differences in detailed phase transition structure, (Cobden *et al.* 2008; Xu *et al.* 2008; Cobden *et al.* 2009) and, consequently, are not considered in this study.

4 BIASES TO AVERAGE STRUCTURE

In most of the mantle, $<V(T, P, X)>$ matches $V<(T, P, X)>$ to within 0.1 per cent (Fig. 6), implying that, in general, seismic structure of the physical reference and horizontally averaged seismic structure agree within the uncertainty range of actual reference seismic models; for AK135, lower-mantle uncertainties are ± 0.1 per cent in V_P and ± 0.15 per cent in V_S, increasing by a factor of 2–5 in the upper mantle (Kennett *et al.* 1995; Cobden *et al.* 2009). Larger differences occur: (i) around phase transitions and (ii) in thermal boundary layers.

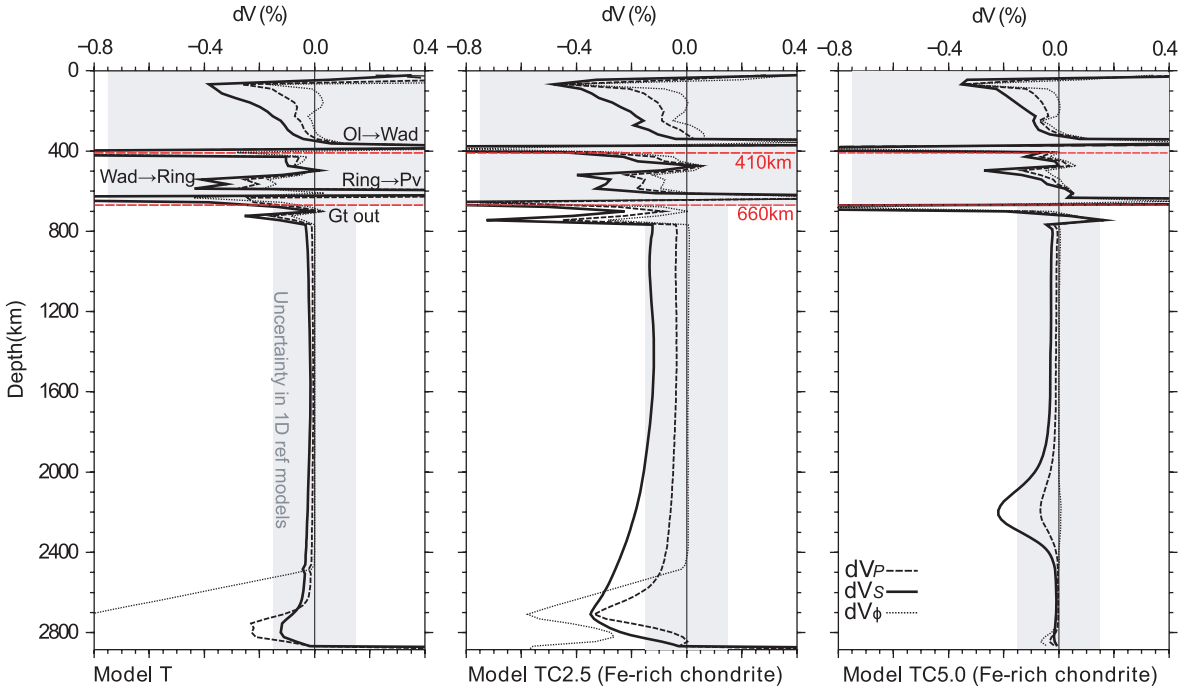

Figure 6. The difference between $<V(T, P, X)>$ (averaged radial velocity) and $V<(T, P, X)>$ (velocity corresponding to the average radial temperature and composition) for the three models. Substantial biases in $<V(T, P, X)>$ develop around phase transitions and, although less pronounced, at thermal boundary layers.

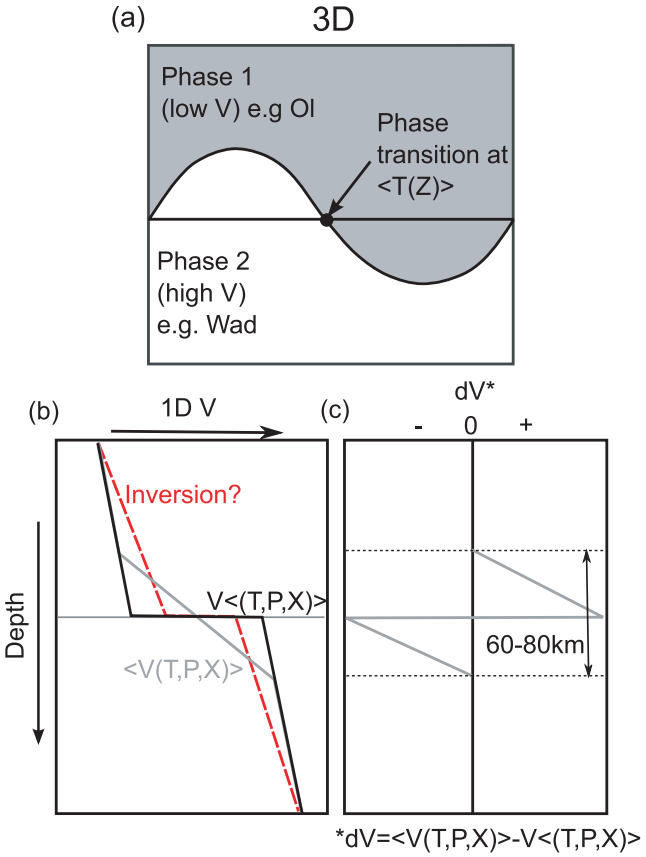

Figure 7. Phase-boundary topography due to lateral variations in temperature (a) cause a broadening of the seismic jump associated with phase transitions along $<V(T, P, X)>$, relative to the jump at $<(T, P, X)>$ (b). This results in sharp peaks in $<V(T, P, X)>-V<(T, P, X)>$ (c). Such peaks may be mapped into elevated gradients (red dashed line) above and below imposed sharp discontinuity depths in 1-D seismic inversions (b).

4.1 Effect of transition topography

Each phase transition is associated with a large positive and negative peak in the difference between the averaged and average structure (Fig. 6). Peaks form because lateral variations in temperature lead to a phase transition that looks broader in the average than it is along the reference physical profile (Fig. 7). While the seismic anomalies arising from lateral temperature variations average out, the phase topography effects themselves do not, because positive and negative anomalies occur at offset depths. The signs of the peaks are always positive above and negative below the equilibrium transition depth because, independent of the sign of the Clapeyron slope, some regions pass through the phase transitions at shallower depth than along the physical reference profile (leading to large local high-velocity anomalies) while others transform at larger depths (leading to local low-velocity anomalies). The width of each peak increases with the magnitude of the Clapeyron slope and with the lateral variation in temperature. The largest peaks for the Ol to Wad and Ring to Pv + Mw transitions have amplitudes of 3–4 per cent and peak widths of 30–40 km.

In the seismic inversions used to infer global 1-D structure (Dziewonski & Anderson 1981; Kennett *et al.* 1995) transition depths and narrow transition widths are prescribed, based on constraints from regional studies. In this case, such biases in averaged structure may map into increased gradients above and below the transitions, and into reduced velocity jumps. A simple calculation indicates that each of these localized, strong velocity anomalies may increase gradients by 10–20 per cent over those along the reference physical structure, and cause a reduction in the jump of a similar magnitude.

Let us consider an example, using some numbers appropriate for the Ol-Wad transition along a 1300 °C adiabat with pyrolitic composition (Cammarano *et al.* 2005a; Cobden *et al.* 2008): assume that at average conditions, the profile has a sharp transition at depth $z_{\rm ref}$ with a 6 per cent increase from V_P of 9 km^{-1}, and velocity gradients of $3 \cdot 10^{-3}$ s^{-1} above and $2 \cdot 10^{-3}$ s^{-1} below. If averaging results in a transition smeared over a region ±30 km around $z_{\rm ref}$, this introduces a traveltime anomaly of –0.05 s above and +0.09 s below $z_{\rm ref}$. If the anomaly accumulated above is mapped into a velocity gradient over a 150-km depth interval above $z_{\rm ref}$, the result is a gradient increase by 10 per cent and a reduction in the jump by 15 per cent. Similar numbers are obtained for the traveltime accrued below $z_{\rm ref}$. A calculation for V_S (jump of 7 per cent from a velocity of 4.8 km s^{-1}, and gradients of $1.2 \cdot 10^{-3}$ s^{-1} above and below) gives traveltime anomalies of –0.11s, and +0.20 s above and below $z_{\rm ref}$, which map into gradients increased by 10–20 per cent, and a jump reduced by 20 per cent. Additional phase transitions as well as the bias in the lithospheric boundary layer (Section 4.2, Fig. 6) could yield cumulative effects of tens of per cent on both gradients and jumps.

Consistent with our interpretation of a potential 3-D bias of phase-transition structure in global reference models, regional studies commonly find larger '410' impedance contrasts (Shearer 2000; Deuss 2009) and often include smaller velocity depth-gradients (e.g. Nolet *et al.* 1994), which is more consistent with the structure expected for an adiabatic-pyrolite mantle. Below '660', however, global 1-D models require velocities higher than in a pyrolitic mantle, which may indicate additional complexity around this transition possibly including vertical chemical gradients (Cobden *et al.* 2008). Further testing into how exactly 3-D biases are mapped into structure in a 1-D seismic inversion is required. However, if the order of magnitude of our calculations is correct, then the biases are similar to the 30 per cent difference in jump at '410' and in predicted gradients for an adiabatic upper mantle and those that are seismically recovered (Li *et al.* 1998; Cammarano *et al.* 2005a; Cammarano & Romanowicz 2007; Cobden *et al.* 2008; Ritsema *et al.* 2009).

4.2 Effect of thermal boundary layers

In all thermal boundary layers, $<V(T, P, X)>$ is lower than the velocity expected for laterally averaged conditions $<(T, P, X)>$. This occurs because the strong temperature dependence of anelasticity increases $\partial V/\partial T$ with temperature. Hence, averaged velocities are always biased towards slower V regions. However, only over large lateral temperature variations does this bias become significant (e.g. over 1000 K in the mantle's upper thermal boundary layer, seismic temperature sensitivities, $\partial V_P/\partial T$ and $\partial V_S/\partial T$, increase by a factor of ∼2 and ∼3. In the lowermost mantle, the increase over a similar ΔT is ∼1.3).

Although chemical heterogeneity is ultimately responsible for mid-mantle boundary layers, the seismic bias introduced has a thermal origin. Biases to the average are almost identical when generated from a seismically fast basaltic or seismically slow Fe-rich composition. This is easily understood: we assume mechanical mixing of compositions and, consequently, the compositional effect on velocity is linear and averages out. The slight effect of chemistry on magnitude of $\partial V/\partial T$ has insignificant effects on the bias between $<V(T, P, X)>$ and $V<(T, P, X)>$.

5 CONCLUSIONS

Our study indicates that 1-D seismic reference models closely reflect the horizontal average thermochemical structure of the mantle. For known composition, an inversion of $<V(T, P, X)>$ for $<T(z)>$ would be correct to within ∼20–30 K, away from phase transitions and thermal boundary layers. In the upper, mid-mantle and lower thermal boundary layers, inversions for $<T(z)>$ could be overestimated by up to ∼40 K, ∼40 K and ∼120 K, respectively.

Biases due to phase-transition topography may help to explain why upper-mantle depth-velocity gradients of 1-D seismic reference models are high, and the jump at '410' low, relative to those expected for an adiabatic pyrolite. This may reduce the need to invoke compositional gradients above and below 400 km depth (Anderson & Bass 1986; Li *et al.* 1998; Cammarano & Romanowicz 2007; Cobden *et al.* 2008; Irifune *et al.* 2008).

Finally, a dense lower-mantle compositional layer with large topography may introduce significant lateral velocity anomalies and a net super-adiabatic thermal gradient. Nonetheless, the radial average physical structure will map, almost without bias, into averaged seismic structure. Hence, chemical heterogeneity may help to reconcile lower-mantle reference *P*- and *S*-wave models.

ACKNOWLEDGMENTS

We thank Ian Jackson and Frederic Deschamps for their thorough and supportive reviews, and Laura Cobden for comments on the manuscript. This research was funded by an STFC postgraduate studentship (ES) and a Research Fellowship from the Royal Commission for the Great Exhibition of 1851 (DRD). Numerical simulations were undertaken on HECToR, the United Kingdom's national high-performance computing service, which is provided by UoE HPCx Ltd. at the University of Edinburgh, Cray Inc and NAG Ltd., and funded by the Office of Science and Technology through EPSRC's High End Computing Programme. DRD also thanks Cyril Hochard, Gerard Stampfli, Huw Davies, Peter Webb and Shell International Exploration & Production, for support with implementing and testing the plate history model utilized herein.

REFERENCES

Anderson, D.L., 1989. Composition of the Earth, *Science,* **243,** 367–370.

Anderson, D.L. & Bass, J.D., 1986. Transition region of the Earth's upper mantle, *Nature,* **320,** 321–328.

Baumgardner, J.R., 1985. Three-dimensional treatment of convective flow in the earth's mantle, *J. Stat. Phys.,* **39,** 501–511.

Bina, C.R. & Silver, P.G., 1990. Constraints on lower mantle composition and temperature from density and bulk sound velocity profiles, *Geophys. Res. Lett.,* **17,** 1153–1156.

Bunge, H.P. & Davies, J.H., 2001. Tomographic images of a mantle circulation model, *Geophys. Res. Lett.,* **28,** 77–80.

Bunge, H.-P., Richards, M.A. & Baumgardner, J.R., 1997. A sensitivity study of three-dimensional spherical mantle convection at 108 Rayleigh number: effects of depth-dependent viscosity, heating mode, and an endothermic phase change, *J. geophys. Res.,* **102,** 11 991–12 007.

Bunge, H.-P., Ricard, Y. & Matas, J., 2001. Non-adiabaticity in mantle convection, *Geophys. Res. Lett.,* **28,** 879–882.

Bunge, H.-P., Richards, M.A. & Baumgardner, J.R., 2002. Mantle-circulation models with sequential data assimilation: inferring present-day mantle structure from plate–motion histories, *Phils. Trans. R. Soc., A,* **360,** 2545–2567.

Cammarano, F. & Romanowicz, B., 2007. Insights into the nature of the transition zone from physically constrained inversion of long-period seismic data, *Proc. Natl. Acad. Sci. USA,* **104,** 9139–9144.

Cammarano, F., Deuss, A., Goes, S. & Giardini, D., 2005a. One-dimensional physical reference models for the upper mantle and transition zone: combining seismic and mineral physics constraints, *J. geophys. Res.,* **110,** B01306, doi:10.1029/2004JB003272.

Cammarano, F., Goes, S., Deuss, A. & Giardini, D., 2005b. Is a pyrolitic adiabatic mantle compatible with seismic data? *Earth planet. Sci. Lett.,* **232,** 227–243.

Cobden, L., Goes, S., Cammarano, F. & Connolly, J.A.D., 2008. Thermochemical interpretation of one-dimensional seismic reference models for the upper mantle: evidence for bias due to heterogeneity, *Geophys. J. Int.,* **175,** 627–648.

Cobden, L. *et al*., 2009. Thermochemical interpretation of 1-D seismic data for the lower mantle: the significance of nonadiabatic thermal gradients and compositional heterogeneity, *J. geophys. Res.,* **114,** B11309, doi:10.1029/2008JB006262.

Connolly, J.A.D., 2005. Computation of phase equilibria by linear programming: a tool for geodynamic modeling and its application to subduction zone decarbonation, *Earth planet. Sci. Lett.,* **236,** 524–541.

Davaille, A., Le Bars, M. & Carbonne, C., 2003. Thermal convection in a heterogeneous mantle, *Comptes Rendus Geosciences,* **335,** 141–156.

Davies, J.H. & Bunge, H.-P., 2001. Seismically fast geodynamic mantle models, *Geophys. Res. Lett.,* **28,** 73–76.

Davies, D.R. & Davies, J.H., 2009. Thermally-driven mantle plumes reconcile multiple hot-spot observations, *Earth planet. Sci. Lett.,* **278,** 50–54.

Deschamps, F. & Tackley, P.J., 2008. Searching for models of thermochemical convection that explain probabilistic tomography I. Principles and influence of rheological parameters, *Phys. Earth planet. Inter.,* **171,** 357–373.

Deschamps, F. & Tackley, P.J., 2009. Searching for models of thermochemical convection that explain probabilistic tomography II: influence of physical and compositional parameters, *Phys. Earth planet. Inter.,* **176,** 1–18, doi:10.1016/j.pepi.2009.1003.1012.

Deschamps, F. & Trampert, J., 2004. Towards a lower mantle reference temperature and composition, *Earth planet. Sci. Lett.,* **222,** 161–175.

Deuss, A., 2009. Global observations of mantle discontinuities using SS and PP precursors, *Surv. Geophys.,* **30,** 301–326.

Duffy, T.S. & Anderson, D.L., 1989. Seismic velocities in mantle minerals and the mineralogy of the upper mantle, *J. geophys. Res.,* **94,** 1895–1912.

Dziewonski, A.M. & Anderson, D.L., 1981. Preliminary reference Earth model, *Phys. Earth planet. Int.,* **25,** 297–356.

Goes, S., Cammarano, F. & Hansen, U., 2004. Synthetic seismic signature of thermal mantle plumes, *Earth planet. Sci. Lett.,* **218,** 403–419.

Irifune, T. *et al*., 2008. Sound velocities of majorite garnet and the composition of the mantle transition region, *Nature,* **451,** 814–817.

Ita, J. & King, S.D., 1994. Sensitivity of convection with an endothermic phase change to the form of governing equations, initial conditions, boundary conditions, and equation of state, *J. geophys. Res.,* **99**(B8), 15 919–915 938, doi:10.1029/1094JB00852.

Ita, J. & King, S.D., 1998. The influence of thermodynamic formulation on simulations of subduction zone geometry and history, *Geophys. Res. Lett.,* **25,** 1463–1466.

Ita, J. & Stixrude, L., 1992. Petrology, elasticity, and composition of the mantle transition zone, *J. geophys. Res.,* **97,** 6849–6866.

Jackson, I., 1998. Elasticity, composition and temperature of the Earth's lower mantle: a reappraisal, *Geophys. J. Int.,* **134,** 291–311.

Jackson, I. & Rigden, S.M., 1998. Composition and temperature of the Earth's mantle: seismological models interpreted through experimental studies of Earth's materials. in *The Earth's Mantle: Composition, Structure and Evolution,* pp. 405–460, ed. Jackson, I., Cambridge University Press, Cambridge, UK.

Jarvis, G.T. & McKenzie, D.P., 1980. Convection in a compressible fluid with infinite Prandtl number, *J. Fluid Mech.,* **96,** 515–583.

Kellogg, L.H., Hager, B.H. & Van Der Hilst, R.D., 1999. Compositional stratification in the deep mantle, *Science,* **283,** 1881–1884.

Kennett, B.L.N., 2006. On seismological reference models and the perceived nature of heterogeneity, *Phys. Earth planet. Inter.,* **159,** 129–139.

Kennett, B.L.N. & Jackson, I., 2009. Optimal equations of state for mantle minerals from simultaneous non-linear inversion of multiple datasets, *Phys. Earth planet. Int.,* **176,** 98–108.

Kennett, B.L.N., Engdahl, E.R. & Buland, R., 1995. Constraints on seismic velocities in the Earth from traveltimes, *Geophys. J. Int.,* **122,** 108–124.

Khan, A., Connolly, J.A.D. & Olsen, N., 2006. Constraining the composition and thermal state of the mantle beneath Europe from inversion of long-period electromagnetic sounding data, *J. geophys. Res.,* **111,** B10102, doi:10.1029/2006JB004270.

Khan, A., Connolly, J.A.D. & Taylor, S.R., 2008. Inversion of seismic and geodetic data for the major element chemistry and temperature of the Earth's mantle, *J. geophys. Res.,* **113,** B09308, doi:10.1029/2007JB005239.

Li, B. & Liebermann, R.C., 2007. Indoor seismology by probing the Earth's interior by using sound velocity measurements at high pressures and temperatures, *Proc. Natl. Acad. Sci. USA,* **104,** 9145–9150.

Li, B., Liebermann, R.C. & Weidner, D.J., 1998. Elastic moduli of Wadsleyite (β-Mg2SiO4) to 7 gigapascals and 873 Kelvin, *Science,* **281,** 675–677.

Mambole, A. & Fleitout, L., 2002. Petrological layering induced by an endothermic phase transition in the Earth's mantle, *Geophys. Res. Lett.,* **29,** 2044, doi:2010.1029/2002GL014674.

Mao, Z. *et al*., 2008. Elasticity of hydrous wadsleyite to 12 GPa: implications for Earth's transition zone, *Geophys. Res. Lett.,* **35,** L21305, doi:21310.21029/22008GL035618.

Matas, J. *et al*., 2007. On the bulk composition of the lower mantle: predictions and limitations from generalized inversion of radial seismic profiles, *Geophys. J. Int.,* **170,** 764–780.

Mattern, E., Matas, J., Ricard, Y. & Bass, J., 2005. Lower mantle composition and temperature from mineral physics and thermodynamic modelling, *Geophys. J. Int.,* **160,** 973–990.

McNamara, A.K. & Zhong, S., 2004. Thermochemical structures within a spherical mantle: superplumes or piles? *J. geophys. Res.,* **109,** B07402, doi:10.1029/2003JB002847.

Mégnin, C. *et al*., 1997. Imaging 3-D spherical convection models: what can seismic tomography tell us about mantle dynamics? *Geophys. Res. Lett.,* **24,** 1299–1302.

Montagner, J.-P., 1994. Can seismology tell us anything about convection in the mantle? *Rev. Geophys.,* **32,** 115–137.

Murnaghan, F., 1951. *Finite Deformation of an Elastic Solid,* Wiley, New York, NY.

Nolet, G., Grand, S.P. & Kennett, B.L.N., 1994. Seismic heterogeneity in the upper mantle, *J. geophys. Res.,* **99,** 23 753–23 766.

Perrillat, J.-P. *et al*., 2006. Phase transformations of subducted basaltic crust in the upmost lower mantle, *Phys. Earth planet. Inter.,* **157,** 139–149.

Ringwood, A.E., 1962. A model for the upper mantle, *J. geophys. Res.,* **67,** 857–867.

Ritsema, J., McNamara, A.K. & Bull, A.L., 2007. Tomographic filtering of geodynamic models: implications for model interpretation and large-scale mantle structure, *J. geophys. Res.,* **112,** B01303, doi:10.1029/2006JB004566.

Ritsema, J., Xu, W., Stixrude, L. & Lithgow-Bertelloni, C., 2009. Estimates of the transition zone temperature in a mechanically mixed upper mantle, *Earth planet. Sci. Lett.,* **277,** 244–252.

Schuberth, B.S.A. *et al*., 2009. Thermal versus elastic heterogeneity in high-resolution mantle circulation models with pyrolite composition: high plume excess temperatures in the lowermost mantle, *Geochem. Geophys. Geosyst.,* **10,** Q01W01, doi:10.1029/2008GC002235.

Shearer, P.M., 2000. *Upper mantle seismic discontinuities American Geophysical Union,* Washington, DC, ETATS-UNIS.

da Silva, C.R.S. *et al*., 2000. The composition and geotherm of the lower mantle: constraints from the elasticity of silicate perovskite, *Phys. Earth planet. Inter.,* **118,** 103–109.

Simmons, N.A., Forte, A.M. & Grand, S.P., 2009. Joint seismic, geodynamic and mineral physical constraints on three-dimensional mantle heterogeneity: implications for the relative importance of thermal versus compositional heterogeneity, *Geophys. J. Int.,* **177,** 1284–1304.

Stampfli, G.M. & Borel, G.D., 2002. A plate tectonic model for the Paleozoic and Mesozoic constrained by dynamic plate boundaries and restored synthetic oceanic isochrons, *Earth planet. Sci. Lett.,* **196,** 17–33.

Stampfli, G.M. & Borel, G.D., 2004. The TRANSMED transects in space and time: constraints on the paleotectonic evolution of the Mediterranean domain, in *The TRANSMED Atlas: the Mediterranean Region from Crust to Mantle,* pp. 53-80, eds Cavazza, W., Roure, F., Spakman, W., Stampfli, G.M. & Ziegler, P., Springer Verlag, Berlin.

Stampfli, G.M. & Hochard, C., 2009. Plate tectonics of the Alpine realm, *Geol. Soc., London, Special Publications,* **327,** 89–111.

Stixrude, L. & Lithgow-Bertelloni, C., 2005. Thermodynamics of mantle minerals–I. Physical properties, *Geophys. J. Int.,* **162,** 610–632.

Sun, S.-S., 1982. Chemical composition and origin of the Earth's primitive mantle, *Geochem. cosmochim. Acta.,* **46,** 179–192.

Tackley, P.J., 1998. Self-consistent generation of tectonic plates in three-dimensional mantle convection, *Earth planet. Sci. Lett.,* **157,** 9–22.

Tackley, P.J., 2002. Strong heterogeneity caused by deep mantle layering, *Geochem. Geophys. Geosyst.,* **3,** 1024, doi:10.1029/2001GC000167.

Tackley, P.J., Stevenson, D.J., Glatzmaier, G.A. & Schubert, G., 1993. Effects of an endothermic phase transition at 670 km depth in a spherical model of convection in the Earth's mantle, *Nature,* **361,** 699–704.

Tackley, P.J., Xie, S., Nakagawa, T. & Hernlund, J.W., 2005. Numerical and laboratory studies of mantle convection: philosophy, accomplishments and thermo-chemical structure and evolution, in *Earth's Deep Mantle: Structure, Composition, and Evolution, Geophysical Monograph Series 160,* pp. 83–99, AGU, Washington, DC, doi:10.1029/1160GM1007.

Tan, E. & Gurnis, M., 2007. Compressible thermochemical convection and application to lower mantle structures, *J. geophys. Res.,* **112,** B06304, doi:06310.01029/02006JB004505.

Trampert, J. & Van Der Hilst, R.D., 2005. Towards a quantitative interpretation of global seismic tomography, *Geophysical Monograph*, **160,** 47–62.

Weidner, D.J., 1985. A mineral physics test of a pyrolite mantle, *Geophys. Res. Lett.,* **12,** 417–420.

Xu, W., Lithgow-Bertelloni, C., Stixrude, L. & Ritsema, J., 2008. The effect of bulk composition and temperature on mantle seismic structure, *Earth planet. Sci. Lett.,* **275,** 70–79.